Front. Struct. Civ. Eng. 2023, 17(1): 122–137
https://doi.org/10.1007/s11709-022-0894-1

RESEARCH ARTICLE

Structural performance of a façade precast concrete sandwich panel enabled by a bar-type basalt fiber-reinforced polymer connector

Junqi HUANG[a,b], Qing JIANG[a,b*], Xun CHONG[a,b], Xianguo YE[a,b], Caihua LIU[a]

[a] *School of Civil and Hydraulic Engineering, Hefei University of Technology, Hefei 230009, China*
[b] *Anhui Civil Engineering Structures and Materials Laboratory, Hefei 230009, China*
[*] *Corresponding author. E-mail: jiangq@hfut.edu.cn*

ABSTRACT In this study, a novel diagonally inserted bar-type basalt fiber reinforced polymer (BFRP) connector was proposed, aiming to achieve both construction convenience and partially composite behavior in precast concrete sandwich panels (PCSPs). First, pull-out tests were conducted to evaluate the anchoring performance of the connector in concrete after exposure to different temperatures. Thereafter, direct shear tests were conducted to investigate the shear performance of the connector. After the test on the individual performance of the connector, five façade PCSP specimens with the bar-type BFRP connector were fabricated, and the out-of-plane flexural performance was tested under a uniformly distributed load. The investigating parameters included the panel length, opening condition, and boundary condition. The results obtained in this study primarily indicated that 1) the bar-type BFRP connector can achieve a reliable anchorage system in concrete; 2) the bar-type BFRP connector can offer sufficient stiffness and capacity to achieve a partially composite PCSP; 3) the boundary condition of the panel considerably influenced the out-of-plane flexural performance and composite action of the investigated façade PCSP.

KEYWORDS precast concrete sandwich panel, basalt fiber reinforced polymer, pull-out performance, shear performance, out-of-plane flexural performance

1 Introduction

Precast concrete has been widely used in construction owing to its short construction period, low labor requirements, and high quality of the fabricated members [1]. The precast concrete sandwich panel (PCSP), as a typical type of precast concrete structural member, primarily comprises an inner and outer reinforced concrete (RC) wythe, core insulation, and connectors that link the two RC wythes. Currently, it has always been used as a façade or load bearing wall. Based on the composite action, PCSPs can be divided into three categories: fully composite, partially composite, and non-composite PCSPs [2]. A fully composite PCSP is one in which the two RC wythes operate together as one panel. A non-composite PCSP has two RC wythes operating independently, and a partially composite PCSP is in between the two extreme mechanical behaviors. Here, the structural performance of the connectors (including the stiffness and strength) and the designed connector spacing in the panels are the main aspects that influence the composite action of a PCSP.

Initially, concrete blocks, steel trusses (i.e., bent-up bars), and steel plates were used as connectors [3]. However, owing to the high thermal conductivity of steel and concrete, a thermal bridge effect would be formed and the energy efficiency of the panel would be significantly reduced. Therefore, fiber reinforced polymer (FRP) materials were introduced to manufacture the connector owing to their low thermal conductivity and high tensile strength [4,5]. Currently, FRP connectors have been designed in different shapes, including the bar-type [6], truss-type [7], plate-type [8–16], grid-type [17–24], and tubular connectors [13,25]. The shear

Article history: Received Dec 31, 2021; Accepted Aug 12, 2022

performance of these connectors is measured using a direct shear test based on a push-out configuration. The out-of-plane flexural performance, including the composite action of the PCSP with the connectors, is evaluated using out-of-plane static load tests.

Currently, the widely used FRP connector in engineering practice is the bar-type connector, which can facilitate an easy construction because it can be directly inserted into the core insulation, while the formed PCSP always reflects a low composite behavior owing to the minor shear stiffness and resistance. The partially composite PCSP always adopts the grid-type and truss-type connector, which can form a truss mechanism, while PCSP with these connectors cannot be constructed as easily as the PCSP with bar-type connector. Therefore, in this paper, a diagonally inserted bar-type basalt FRP (BFRP) connector is proposed, which aims to achieve both construction convenience and partially composite behavior. The geometrical dimensions of the BFRP bar are 8 mm × 150 mm (diameter × length), and a diagonal collar is installed on the bar (Fig. 1). Meanwhile, the BFRP bar is sand-coated and helically wrapped by the multifilament yarn to improve the bond between the connector and concrete [26].

A façade wall panel is always subjected to an out-of-plane wind and seismic load during its service life. In engineering practice, for tall buildings in China, the connection often used between a façade PCSP and the main structure (e.g., precast RC frame) is shown in Fig. 1, in which the top of the façade PCSP is connected with the top RC beam through the connecting steel rebar; the bottom of the façade PCSP is connected with the bottom RC beam through steel angles. Currently, the out-of-plane flexural performance of the façade PCSP is always studied using the four-point flexural loading test in which the PCSP is fully considered as a one-way element [12]. However, when the PCSP is enabled by the aforementioned practical boundary condition, it behaves as a two-way element, and the out-of-plane flexural performance (e.g., cracking load, crack pattern) would differ from that of the one-way element. Currently, information on this aspect is lacking.

Thus, in this study, first, the pull-out performance of the bar-type BFRP connector in concrete after the exposure to different temperatures was investigated through a pull-out test. Thereafter, the shear performance of the bar-type BFRP connector was investigated through the in-plane direct shear test. Finally, five façade PCSP specimens were fabricated and tested under a uniformly distributed load with the simulated boundary condition in Fig. 1. The investigating parameters primarily consisted of the length of the panel, opening condition, and boundary condition. The main objectives of this study were to 1) evaluate the performance of the connector's anchorage system at different service temperatures; 2) confirm the potential of the connector to achieve the partially composite PCSP; 3) study the effect of the aforementioned investigated parameters on the out-of-plane flexural performance of the façade PCSP.

2 Pull-out performance of bar-type basalt fiber reinforced polymer connector in concrete

2.1 Details of the specimens

The pull-out performance of the bar-type BFRP connector in concrete after the exposure to different temperatures (i.e., –20, 0, 25, 40, and 60 °C) was evaluated first using the pull-out test. Here, –20 °C is below the lowest temperature in the most regions of China [27]. Moreover, the surface a façade reinforced concrete wall panel can reach approximately 60 °C under

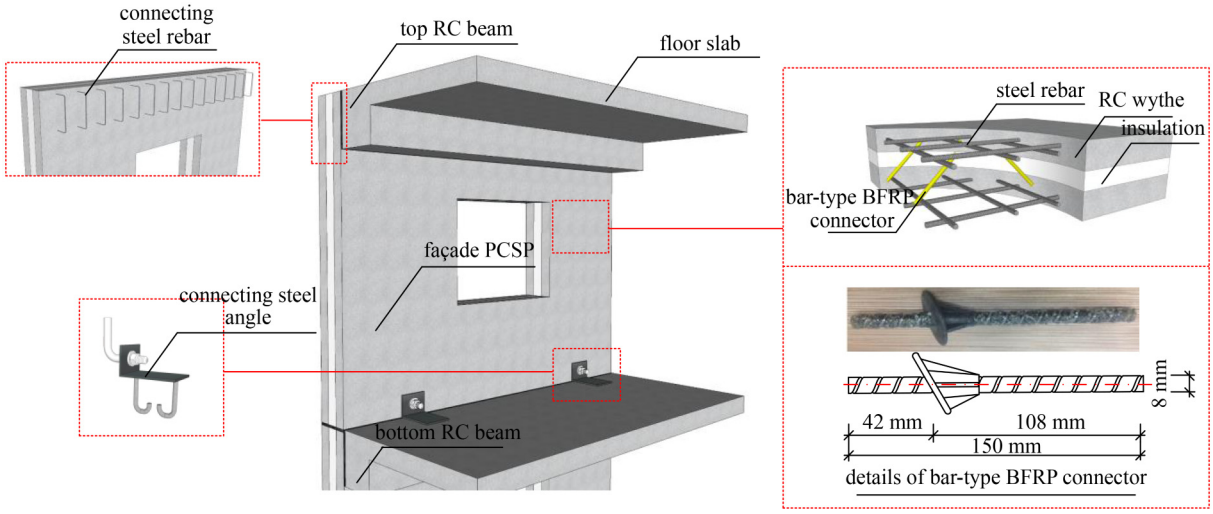

Fig. 1 Façade PCSP and the proposed connector.

a sunny weather in summer [28]. The tested bar-type BFRP connector was a sand-coated ribbed type with a diameter of 8 mm (Fig. 1). The material properties of the connector are given in Table 1. Figure 2(a) shows the configuration of the pull-out specimen, in which the connector was embedded in a concrete cube with dimensions of 250 mm × 250 mm × 250 mm (length × width × height). The embedded length was 42 mm. The tested concrete cube strength of the specimens was 41.7 MPa. Four identical specimens were prepared for each temperature level. The specimens were termed in the form of ST-T-1/2/3/4, where "T" refers to the tested temperature ("0", "25", "40", and "60" °C); and "B20" represents –20 °C.

2.2 Test procedure

All specimens were cured under ambient temperature for more than 90 d. Thereafter, the specimens were moved into an electrical temperature furnace. The furnace was then heated or cooled into the target temperature at a rate of 20 °C/min, and the target temperature was maintained for 1 h. Thereafter, the specimens were cooled naturally to room temperature, and the pull-out test was conducted using a universal testing machine. During the pull-out test, a load was applied to the specimen through displacement control, and a loading rate of 1 mm/min was adopted, which was designed according to Ref. [29]. One linear variable differential transformer (LVDT) was placed to measure the pull-out distance. Here, two specimens (i.e., ST-25-4 and ST-40-4) were damaged during de-molding. Thus, a total of 18 specimens were tested in this study.

2.3 Test results and discussion

2.3.1 Load–displacement relationship and failure mechanism

The relationships between load and displacement are shown in Figs. 2(b)–2(f), and the general shape of all curves is shown in Fig. 2(g). For all specimens, the curves could be divided into four stages. Initially (i.e., OA stage in Fig. 2(g)), the load increased linearly with the displacement. Thereafter (i.e., AB stage in Fig. 2(g)), the slope of the curve gradually decreased until the peak load level, which was the pull-out capacity of the specimens. In the third stage (i.e., BC stage in Fig. 2(g)), a sudden decrease in the curve was observed, which indicated the failure initiation of the specimens. Finally (i.e., CD stage in Fig. 2(g)), the decrease in the curves became moderate and the load almost approached zero, indicating the complete failure of the specimens.

Generally, the bond between concrete and connector consists of the chemical bond, friction force, and interlock force caused by the rib and surrounding concrete [30]. In the first stage (i.e., OA stage), the bond primarily consisted of the chemical bond and static friction, and the slip was marginal. In the second stage (i.e., AB stage), with an increase in the load, these two actions gradually degraded owing to the micro-slip between the connector and concrete. In the meantime, the mechanical interlock between the connector rib and surrounding concrete increased, and this mechanical interlock governed the bond mechanism. Here, conical surface cracks were observed in the specimens when the tensile force reached the peak level. Thereafter (i.e., BC stage), the crack became wider, which indicated the failure of the mechanical interlock, and the tensile force decreased sharply. Eventually (i.e., CD stage), only the sliding friction force existed, which formed the residual force of the curve. For all specimens, a conical shaped concrete was pulled out with the connector; the typical failure mode of the specimens is shown in Fig. 2(g).

Table 1 Material properties of the steel rebar and BFRP connector used in this study

ID	diameter (mm)	E_r (GPa)	f_y (MPa)	ε_y	f_u (MPa)
bar-type BFRP connector	8	49	–	–	1055
D6 steel rebar	6	200	452	0.00226	600
D10 steel rebar	10	200	455	0.00228	618

Note: E_r is the elastic modulus of the rebar; f_y is the yielding stress of the rebar; ε_y is the strain at the yielding stress; f_u is the maximum stress of the rebar.

2.3.2 Effect of temperature on the pull-out capacity

The pull-out capacity of each specimen is shown in Fig. 2(h) and Table 2, and the average value in each temperate level is shown in Table 2. Generally, by increasing the temperature from –20 to 60 °C, the pull-out capacity exhibited a decrease of 50.8%, i.e., from 17.9 to 8.8 kN. This was probably because the mechanical property of the resin was deteriorated with the increase in temperature, which lowered the mechanical interlock action. In addition, as shown in Fig. 2(h), the pull-out capacity decreased almost linearly with the increase in temperature, although the data were scattered. Based on the data in Fig. 2(h), linear regression analysis was conducted and the relationship between the pull-out capacity and temperature was obtained as Eq. (1). The coefficient of determination of the equation (R^2) was 0.87:

$$P_{po} = -0.1105T + 16.139, \quad (1)$$

where P_{po} is the pull-out capacity of the bar-type BFRP connector (kN); T is the exposure temperature (°C).

The predicted pull-out capacities using Eq. (1) are shown in Table 2. A good correlation was observed between the test and predicted results, in which the ratio

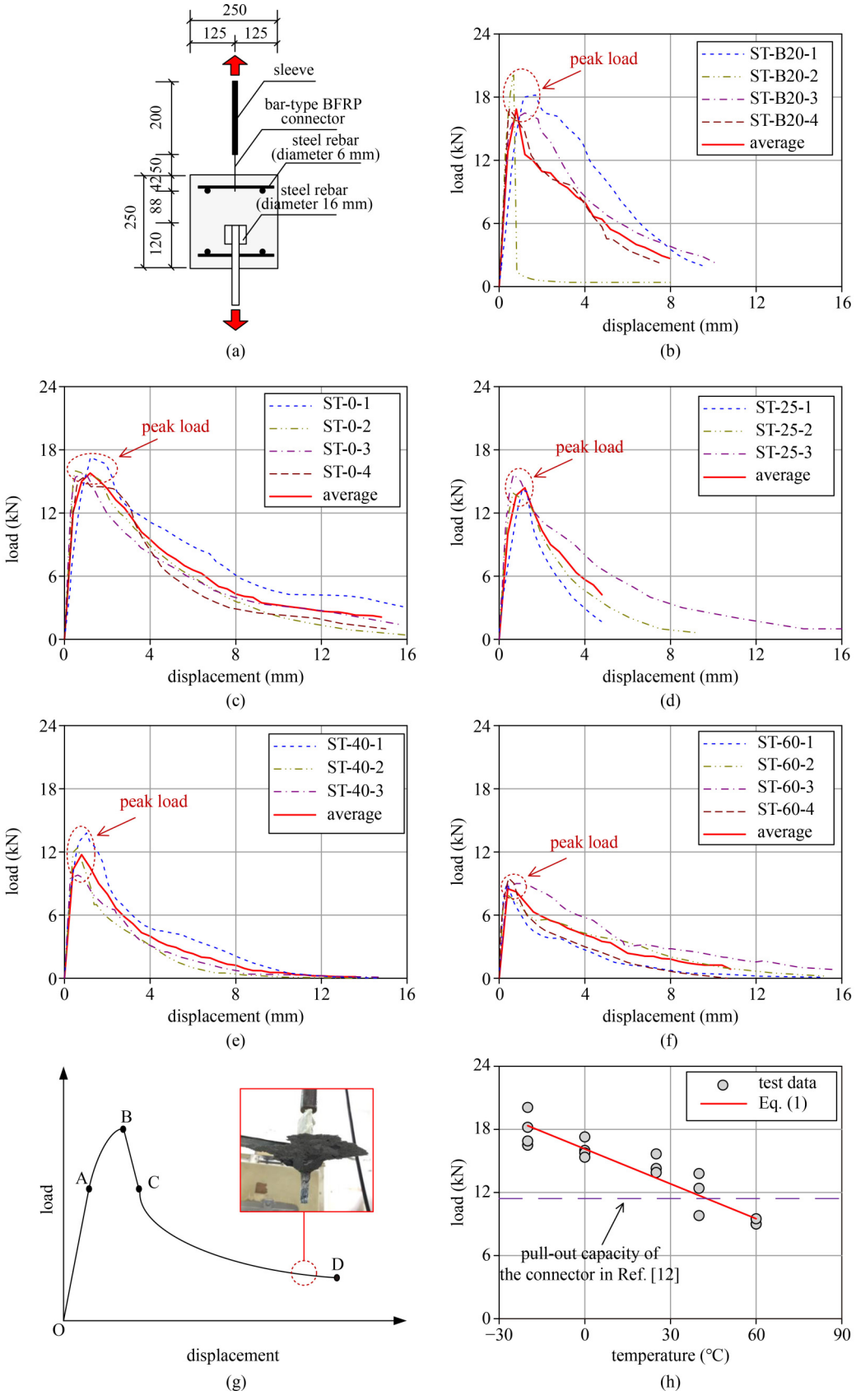

Fig. 2 Pull-out test of the connector: (a) dimensions of the specimen (unit: mm); (b) ST-B20 specimens; (c) ST-0 specimens; (d) ST-25 specimens; (e) ST-40 specimens; (f) ST-60 specimens; (g) shape of the curves and failure mode; (h) relationship between pull-out capacity and temperature.

Table 2 Pull-out capacities of the test specimens

specimen ID	embedded length (mm)	temperature (°C)	pull-out capacity (kN)			
			test (individual)	test (average)	predicted using Eq. (1)	test/predicted ratio
ST-B20-1	42	–20	18.2	17.9	18.3	0.98
ST-B20-2	42	–20	20.1			
ST-B20-3	42	–20	16.5			
ST-B20-4	42	–20	16.9			
ST-0-1	42	0	17.3	16.1	16.1	1.00
ST-0-2	42	0	16.0			
ST-0-3	42	0	15.8			
ST-0-4	42	0	15.4			
ST-25-1	42	25	14.3	14.6	13.4	1.09
ST-25-2	42	25	13.9			
ST-25-3	42	25	15.7			
ST-40-1	42	40	13.8	12.0	11.7	1.02
ST-40-2	42	40	12.4			
ST-40-3	42	40	9.8			
ST-60-1	42	60	9.0	8.8	9.5	0.93
ST-60-2	42	60	7.8			
ST-60-3	42	60	9.0			
ST-60-4	42	60	9.5			

between test and predicted results was 0.93–1.09. Moreover, the pull-out capacity of a plate-type FRP connector previously investigated by the author of this study [12] was compared with that of the bar-type BFRP connector (see Fig. 2(h)); the bar-type BFRP connector presented a higher pull-out capacity at the exposure temperature of –20–40 °C, indicating a reliable anchorage system of this connector.

3 Direct shear test of the bar-type basalt fiber reinforced polymer connector

3.1 Details of the test specimens

A direct shear test was conducted to evaluate the performance of the bar-type BFRP connector. Here, three identical direct shear test specimens were fabricated and tested. The geometrical dimensions of the specimens were 1215 mm × 500 mm × 600 mm (height × length × width). The specimens consisted of two 100 mm thick exterior RC wythes, one 200 mm core RC wythe, and two 50 mm thick smooth surface extruded polystyrene (XPS) insulation boards, representing two PCSPs back-to-back. The authors validated that the bond between the concrete and this type of the insulation almost had no effect on the shear transfer mechanism of the PCSP [13]. Each concrete wythe consisted of two layers of the reinforcement mesh, in which both longitudinal and transverse steel rebar had a diameter of 6 mm and were placed with a spacing of 150 mm. The material properties of the rebar are shown in Table 1. The specimen consisted of four bar-type BFRP connectors with two in each side to form a truss mechanism (Fig. 3(a)). During fabrication, three 150 mm × 150 mm × 150 mm concrete cubes were reversed to measure the concrete compressive strength of the specimens, and the tested 28-d strength was 38.7 MPa.

The specimens were tested using in-plane direct shear. The load was added through a hydraulic jack. Before the peak shear load, the applied load was controlled according to force at 2 kN intervals. When the load reached the descending stage, it was controlled according to displacement at 2 mm intervals. Two LVDTs were placed at the front and back of the specimens to measure the relative slip between the core and exterior RC wythe.

3.2 Test results and discussion

The shear force–relative slip relationship of the individual specimens and average response are shown in Fig. 3(b). Similar to Fig. 2(g), the curve could be divided into four stages: initial linear increase, non-linear increase until the peak load, sudden drop, and moderate descending. The peak shear load of the specimens was 39–43 kN, with an average value of 41 kN.

The shear force of the specimen was primarily contributed by the tension and compression of the bar-

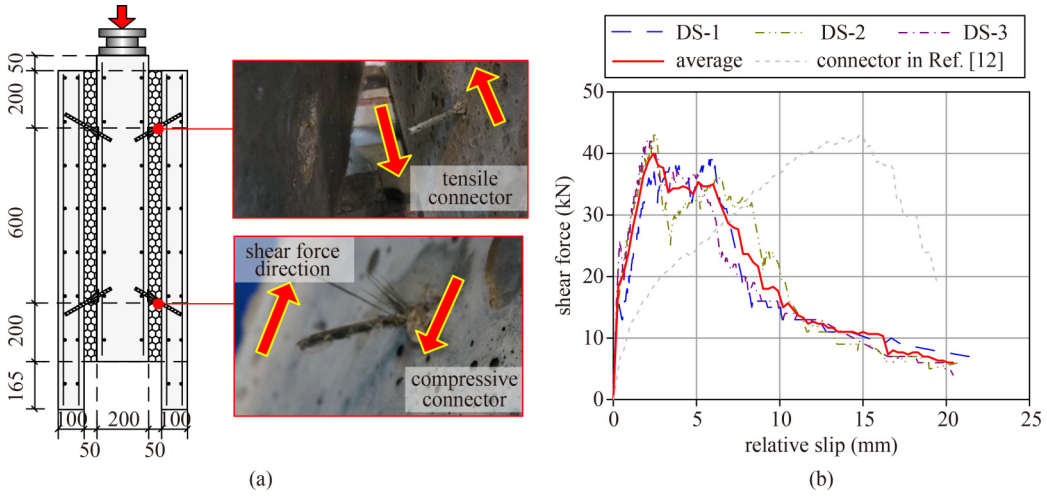

Fig. 3 Direct shear test of the specimen: (a) test specimen and failure mode; (b) shear force–relative slip relationship.

type BFRP connector and the bond between the insulation and concrete. Here, at the end of the initial linear increase stage, the bond between insulation and concrete began to be damaged, and the resin of FRP began to be damaged. Thus, a non-linear increase stage was formed. At the peak load level, the conical surface cracks formed in the concrete at the tensile bar-type BFRP connector, indicating a pull-out failure. For the compressive bar-type BFRP connector, FRP crushing was initiated. Therefore, a sudden loss of the reaction force was observed. Eventually, the residual shear force was primarily contributed by the sliding friction between the tensile bar-type BFRP connector and concrete and the compression of the compressive bar-type BFRP connector. The failure mode of the specimen was governed by the pull-out of the tensile BFRP connector and the FRP crushing of the compressive BFRP connector (Fig. 3(a)).

Previously, the authors investigated a plate-type FRP connector that could form a partially composite PCSP [12]. The shear force–relative slip relationships of the specimens are compared in Fig. 3(b). Here, the bar-type BFRP connector reflected a higher stiffness, and the peak shear loads of the two types of the connectors were almost equal. Therefore, the investigated bar-type BFRP connector offered a good potential to achieve a partially composite action in the PCSP.

4 Out-of-plane flexural performance of the precast concrete sandwich panel

4.1 Test specimens

A total of five façade PCSP specimens were fabricated at Changsha Broad Homes Industrial Group Co., Ltd (Anhui Branch), and they were all designed according to an actual precast residential building project in Hefei, China. Initially, the steel mould was installed and the steel reinforcement of the bottom RC wythe was placed (Fig. 4(a)). Thereafter, the concrete was poured to form the bottom RC wythe (Fig. 4(b)), followed by covering the XPS insulation, inserting the BFRP connectors, and installing the top wythe steel reinforcement (Fig. 4(c)). Finally, the top wythe concrete was poured to form the final configuration of the PCSP (Fig. 4(d)).

The thickness of the XPS insulation, inner and outer RC wythes were 50, 50, and 60 mm, respectively. The height of all wall specimens was 2930 mm. According to design method in Refs. [1,2], the calculated maximum thermal bow was 2 mm when the outdoor and indoor temperature difference was 30 °C, and it was significantly lower than the deflection at the service limit state (i.e., span/360 = 8.1 mm). The concrete cover remained at 20 mm. The spacing between the BFRP connectors was 600 mm, in both longitudinal and transverse directions. The longitudinal and transverse steel rebar had a diameter of 10 mm and was placed at a spacing of 150 mm. The material property of the steel rebar is shown in Table 1. The cube strength of the concrete used for the PCSP at the test date was 53.2 MPa.

The PCSP specimens were tested according to the boundary condition (i.e., connection type) in Fig. 1. Note that the rotation restraint of the top and bottom connection in Fig. 1 was weak. Thus, in this study, all PCSP specimens were simply supported as shown in Fig. 5, which was according to the simplified boundary condition in Ref. [31]. Here, the top edge of the specimen was supported by the steel rod and the bottom edge of the specimen was supported by the steel ball (Figs. 5(b) and 5(c)).

The investigating parameters of the five PCSP specimens included the length of the panel (4980, 6280, and 8020 mm), number of the openings (with two openings and without opening), and number of the steel ball supports (2, 3, and 4). Details of the specimens are provided in Table 3 and Fig. 6. The specimen was termed

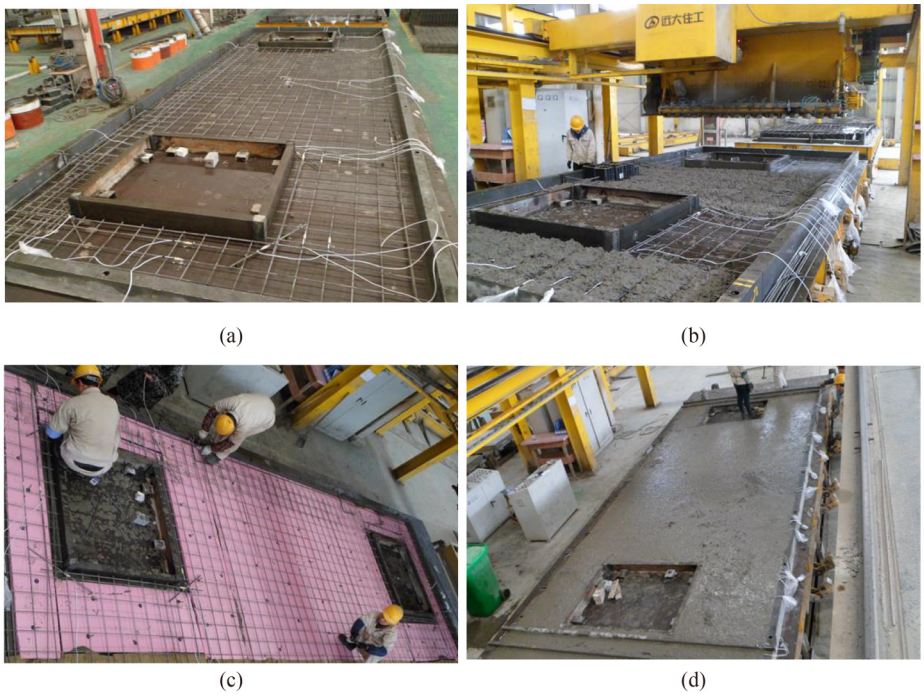

Fig. 4 Fabrication process of the PCSP specimens in this study: (a) installing the bottom layer reinforcement; (b) pouring bottom layer concrete; (c) installing the XPS insulation, connector, and top layer reinforcement; (d) pouring top layer concrete.

in the form of SP-L-O-S, in which "L" refers to the length of the specimen (i.e., "4980", "6280", and "8020"), "O" refers to the opening number of the specimen, (i.e., "0" and "2"), and "S" refers to the number of the steel ball support ("2", "3", and "4").

LVDTs were used to measure the deflection of the specimens. Strain gauges were attached on the reinforcements, which were expected to exhibit a relatively high tensile strain (i.e., those at the mid-span between the bottom supports, the mid-height of the panel, and the corner of the opening), as shown in Fig. 6. A load was applied by adding steel blocks (10 kg each) on the top surface of the specimens, aiming to simulate a uniformly distributed wind load, which followed the similar loading method in Ref. [32]. In addition, for the specimens with openings, steel sheet with 10 mm thick was used to cover the opening to place the steel block. Note that for safety, the test was terminated when any rebar strain reached 0.002 and the maximum crack width reached 0.4 mm.

4.2 Test results

4.2.1 Crack pattern

The crack pattern of all specimens are shown in Fig. 7. For SP-4980-0-2 (Fig. 7(a)), the first crack occurred at 3 kN/m^2 and propagated in the longitudinal direction (i.e., along the panel height). For SP-4980-0-3 (Fig. 7(b)), the first crack occurred at 7 kN/m^2 and propagated in the transverse direction (i.e., along the panel length). For the specimens with openings (Figs. 7(c)–7(e)), the first crack occurred at the corner of the opening, and the cracking loads were 3.0, 1.0, and 2.0 kN/m^2 for SP-6280-2-3, SP-8020-2-3, and SP-8020-2-4, respectively. A possible reason was that the stress concentration existed in the corner of the opening, which induced a significant higher stress than other areas and resulted in a lower cracking load of the entire panel. As the load increased, tangential cracks occurred at the bottom steel ball support for most of the specimens. Here, for SP-6280-2-3, the tangential crack was not apparent.

4.2.2 Load–deflection relationship

The relationship between the applied load and deflection at the center point of the specimen is shown in Figs. 8(a)–8(e). In the figure, the curves are compared with those of the fully composite (FC) and non-composite (NC) counterparts, which were obtained through finite element (FE) analysis. The tested curves are also compared in Fig. 8(f). Generally, for all specimens, the curve could be divided into two or three typical stages. In the first stage (0 to cracking load), the load increased almost linearly with the deflection. Thereafter, (cracking load to yielding load), the slope of the curve decreased slightly, and a non-linear increase stage occurred. For SP-4980-0-2 and SP-8020-2-4, the test was terminated before an apparent yielding plateau occurred. For the other three specimens, a third stage was observed (yielding load to

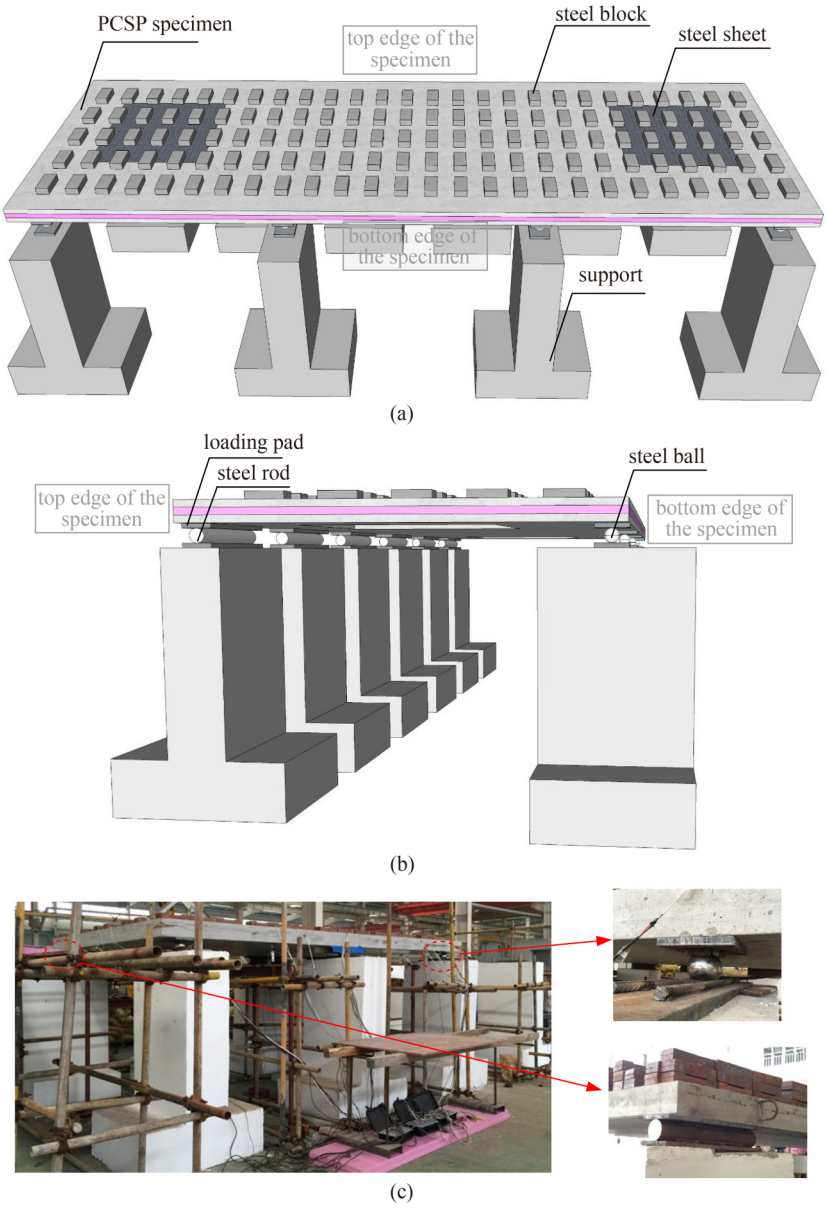

Fig. 5 Details of the flexural test setup: (a) details of the test setup; (b) boundary condition of the flexural test specimen; (c) photo of the test setup.

Table 3 Details of the flexural test PCSP specimens

specimen ID	length (mm)	height (mm)	thickness (mm)	connector spacing (mm)	opening number	bottom support number	bottom support spacing (mm)
SP-4980-0-2	4980	2930	160 (60-50-50)	600	0	2	4350
SP-4980-0-3	4980	2930	160 (60-50-50)	600	0	3	2175
SP-6280-2-3	6280	2930	160 (60-50-50)	600	2	3	2780
SP-8020-2-3	8020	2930	160 (60-50-50)	600	2	3	3675
SP-8020-2-4	8020	2930	160 (60-50-50)	600	2	4	2400 and 2550

termination), in which the slope of the curve significantly dropped and the yielding plateau emerged. Furthermore, for all specimens, the test load–deflection relationships lay between the corresponding FC and NC curves, indicating a partially composite action for the specimens.

4.2.3 Load–strain relationship

The load–strain relationships of all test specimens are shown in Fig. 9. The selected strain gauge was the one with the largest strain value (i.e., first yielded point).

Generally, a significant reduction in the slope of the curve was observed after the specimen cracked. Herein, for SP-4980-0-2 and SP-8020-2-3, the first yielded point was at the mid-span between the bottom supports. By adding the bottom support, the first yielded point moved to the mid-height of the specimen (i.e., SP-4980-0-3 and SP-8020-2-4). For SP-6280-2-3, the first yielded point was at the corner of the opening.

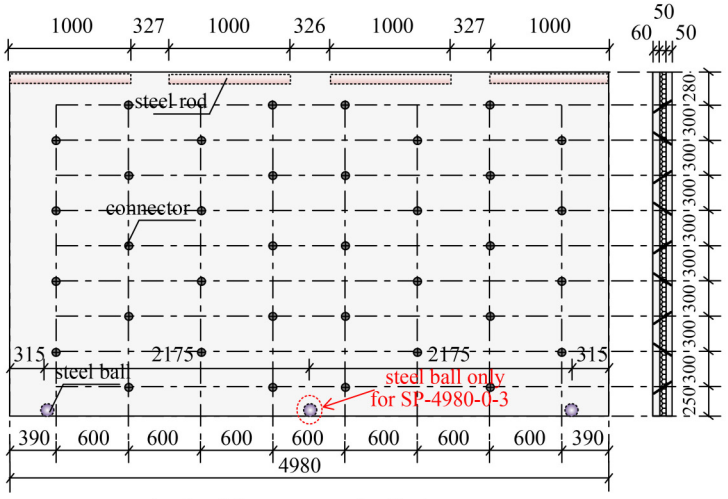

details of the connector distribution

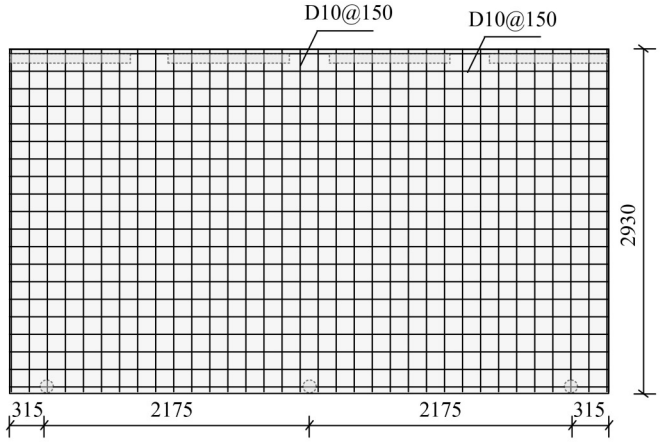

details of the reinforcement

(a)

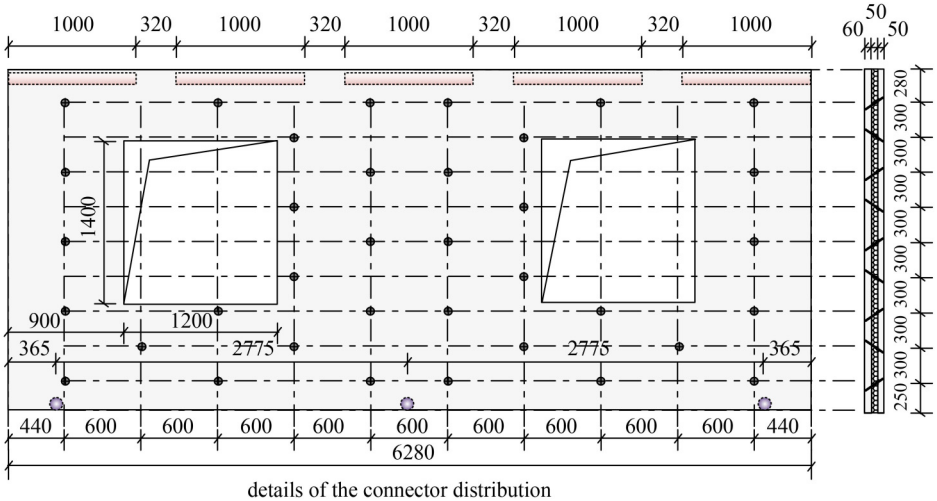

details of the connector distribution

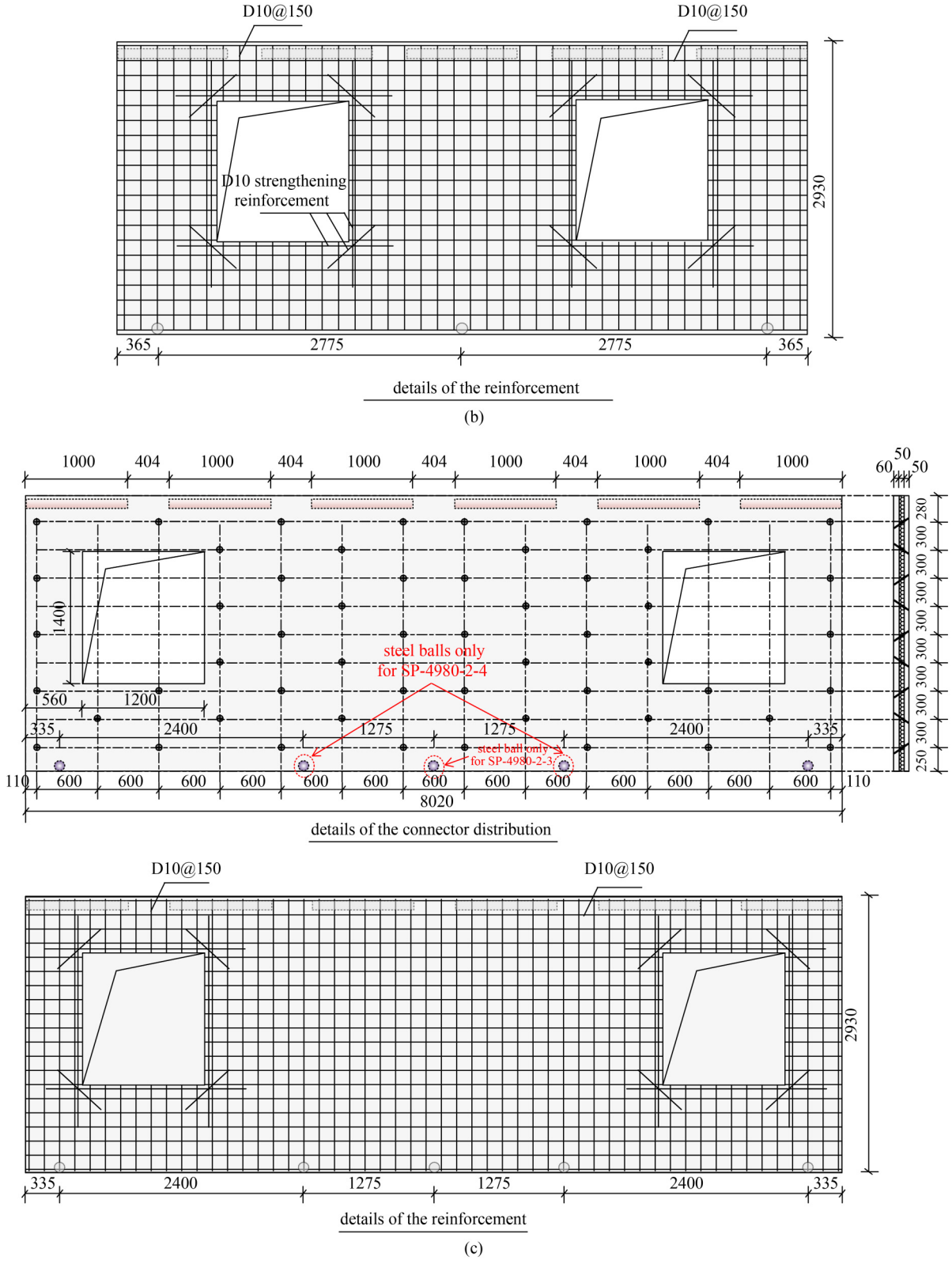

Fig. 6 Geometrical dimensions of the SP specimens (unit: mm): (a) SP-4980-0-2 and SP-4980-0-3; (b) SP-6280-2-3; (c) SP-8020-2-3 and SP-8020-2-4.

4.2.4 Effect of the investigating parameters

The cracking load, and the initial slope (denoted as "K_i") of the tested load–deflection curve in Fig. 8 are shown in Table 4. Here, the effects of the investigating parameters including the length of the panel, number of the openings,

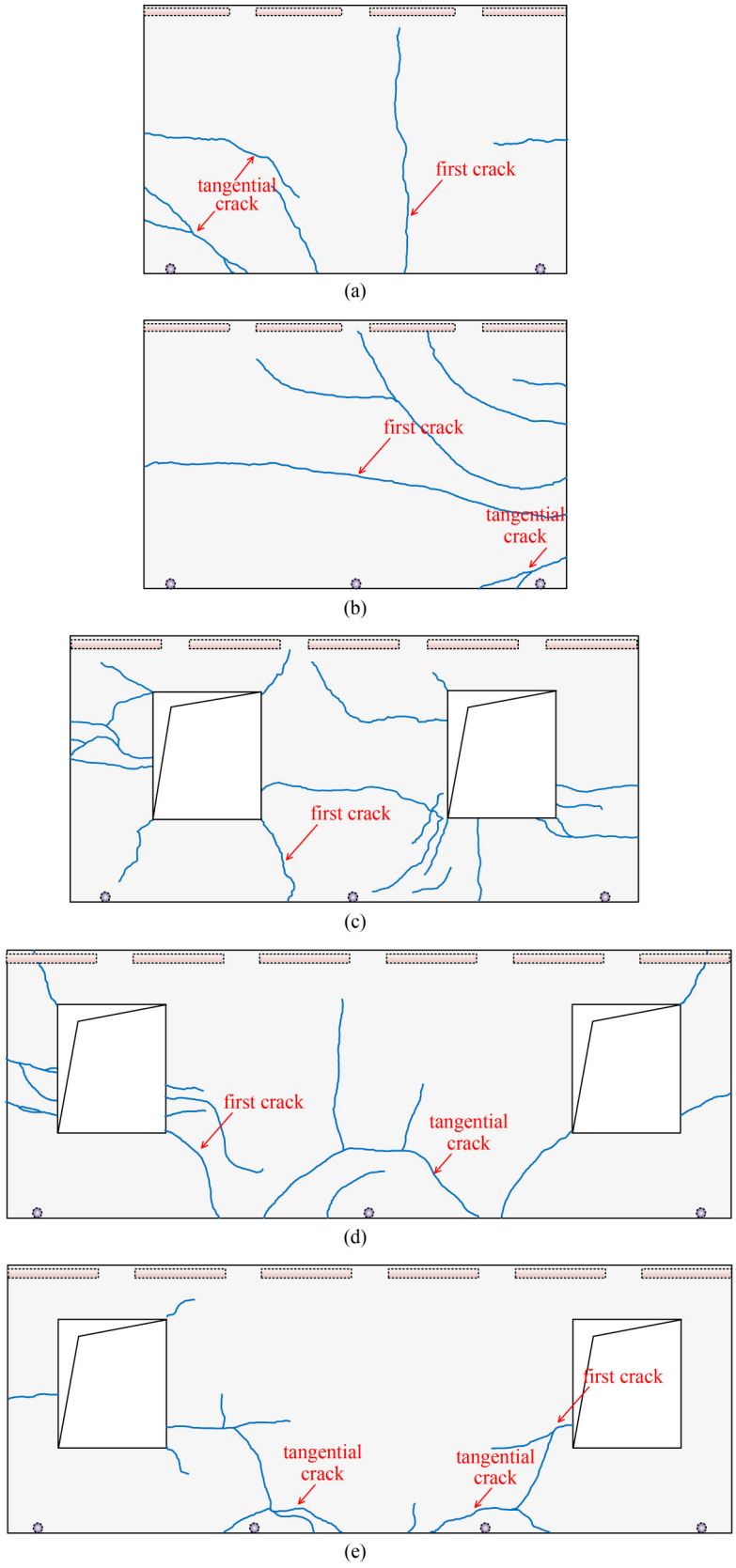

Fig. 7 Crack pattern of the test specimens: (a) SP-4980-0-2; (b) SP-4980-0-3; (c) SP-6280-2-3; (d) SP-8020-2-3; (e) SP-8020-2-4.

and number of bottom supports on the flexural performance of the panel were as follows.

1) Effect of the bottom support number: increasing the bottom support number (i.e., reducing the bottom support

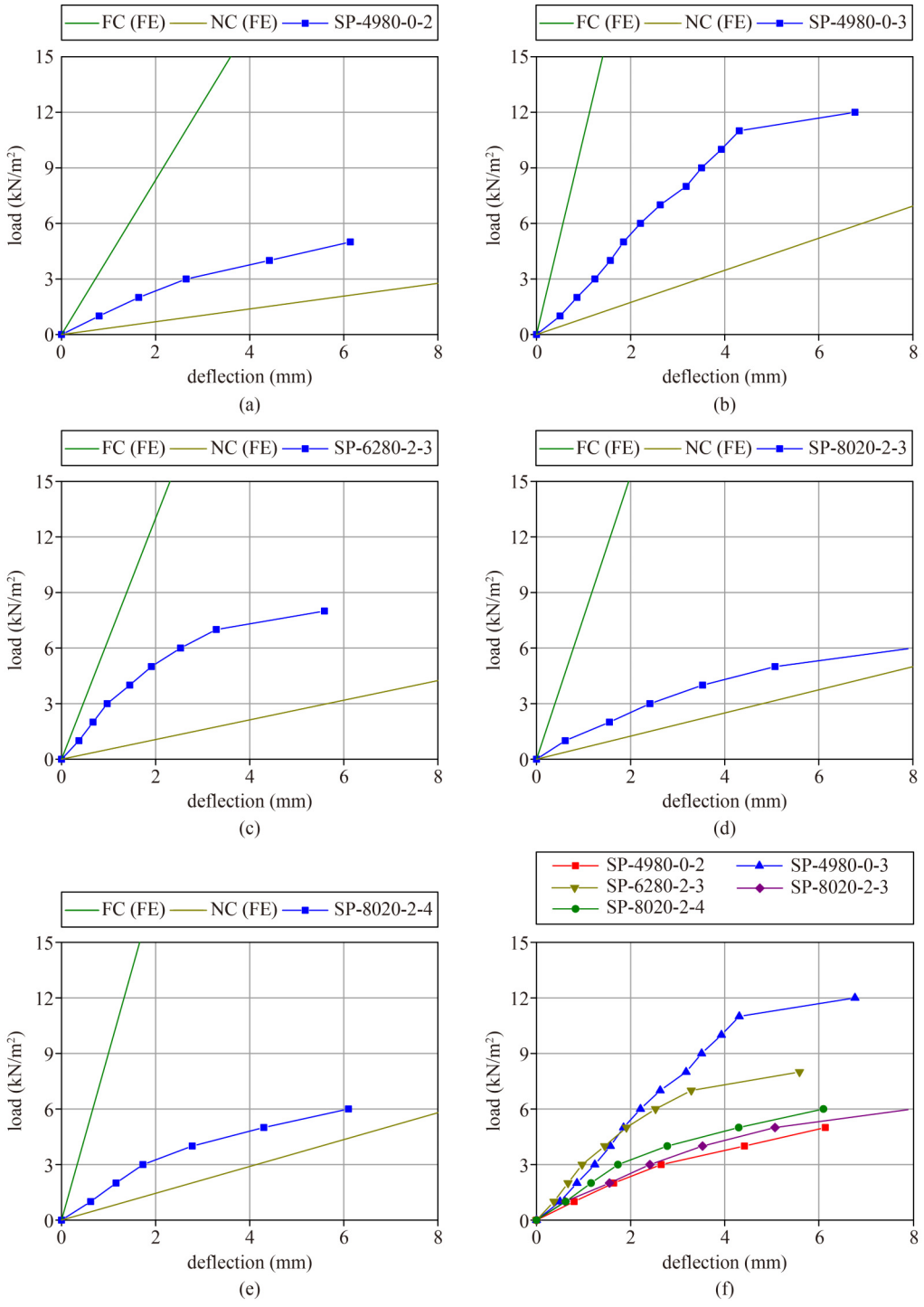

Fig. 8 Load–deflection relationship of the PCSP specimens: (a) SP-4980-0-2; (b) SP-4980-0-3; (c) SP-6280-2-3; (d) SP-8020-2-3; (e) SP-8020-2-4; (f) comparison between different specimens.

spacing) significantly improved the cracking load and K_i. This was primarily because the boundary condition significantly influenced the internal force transfer mechanism of the entire panel. Herein, comparing the test results between SP-4980-0-2 and SP-4980-0-3, we observed that by increasing the bottom supports from 2 to 3 (i.e., reducing the spacing from 4350 to 2175 mm), an increase of 133% and 60% was observed on cracking load and K_i, respectively (i.e., from 3 to 7 kN/m^2 and from 1250 to 2000 kN/m^3). Moreover, comparing the test results of SP-8020-2-3 and SP-8020-2-4, we observed that that the cracking load and K_i exhibited increases of 100% and 5%, respectively (i.e., from 1 to 2 kN/m^2 and from 1639 to 1724 kN/m^3), through increasing the bottom support from 3 to 4 (i.e., reducing the spacing from 3675 to 2550 mm). In addition, by adding support, the

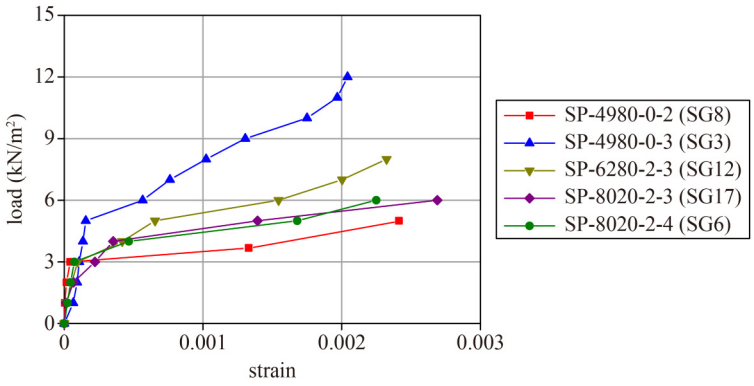

Fig. 9 Load–strain relationship of the specimens.

Table 4 Cracking load, initial curve slope, and degree of composite action of the specimens

specimen ID	P_{cr} (kN/m^2)	K_i (kN/m^3)	Δ_{test} (mm)	Δ_{fully} (mm)	Δ_{non} (mm)	DCA_d (%)
SP-4980-0-2	3.00	1250	0.80	0.24	2.89	78.87
SP-4980-0-3	7.00	2000	0.50	0.09	1.15	61.68
SP-6280-2-3	3.00	2703	0.37	0.15	1.88	87.50
SP-8020-2-3	1.00	1639	0.61	0.13	1.60	67.41
SP-8020-2-4	2.00	1724	0.58	0.11	1.38	63.02

Note: P_{cr} is the cracking load; K_i is the initial slope of the load-deflection curve; Δ_{test} is the deflection of the tested PCSP at a selected load level; Δ_{fully} is the corresponding deflection of the fully composite PCSP; and Δ_{non} is the corresponding deflection of the non-composite PCSP.

longitudinal crack on the PCSP decreased owing to the change in the internal force transfer mechanism.

2) Effect of the specimen length: under a certain bottom support number, increasing the panel length enlarged the bottom support spacing. Therefore, the cracking load and K_i decreased. Herein, comparing the test results between SP-6280-2-3 and SP-8020-2-3, by increasing the length from 6280 to 8020 mm, the cracking load and K_i decreased by 33% and 36%, respectively (i.e., from 3 to 2 kN/m^2 and from 2703 to 1724 kN/m^3).

3) Effect of the opening: the opening condition appeared to particularly affect the crack pattern of the specimen based on the comparison of the test results. For the specimens with openings, the crack initiated at those opening corners owing to the stress intensity.

4.3 Assessment of the composite actions

The initial flexural performance of the FC and NC PCSPs was obtained through the FE analysis. Thereafter, the degree of composite action of all specimens was calculated and analyzed.

4.3.1 Initial flexural performance of fully composite and non-composite precast concrete sandwich panels

The initial flexural performance of the FC and NC PCSPs was obtained through the general-purpose FE software ABAQUS [33]. For the modelling method, the three-dimensional four-node shell element (S4R) was used for the concrete panel and steel sheet that covered the opening to transfer the distributed load. The steel reinforcement fiber was added through the "*Rebar" command into the shell element, which indicates a perfect bond between the concrete and steel rebar. The element size was adopted as 100 mm according to a convergence study prior to the analysis. The elastic modulus and Poisson's ratio of the concrete were adopted as $4700f_c^{0.5}$ [34] and 0.2, respectively, where f_c is the cylinder strength of concrete and can be obtained using $f_c = 0.76f_{cu}$ (f_{cu} is the concrete cube strength). For the steel rebar, these values were 200 GPa and 0.2, respectively.

The analysis method was verified using a 3000 mm × 1000 mm × 170 mm (length × width × thickness) solid RC panel flexural test previously conducted by the author [12]. The comparison between the predicted and tested load–deflection relationships are shown in Fig. 10(a), and a good agreement was observed. Based on the validated model, the initial flexural performance of the FC and NC PCSP was simulated, and a typical FE model is shown in Fig. 10(b). The obtained load–deflection relationships are shown in Figs. 8(a)–8(e). The load–deflection relationship of the fully composite PCSP was obtained by analyzing the 160 mm thick solid façade RC panel. Moreover, the load–deflection relationship of the non-composite PCSP was obtained as the sum of the analysis results of two independent RC wythes. Figures 8(a)–8(e) show that all specimens reflected a partially composite action.

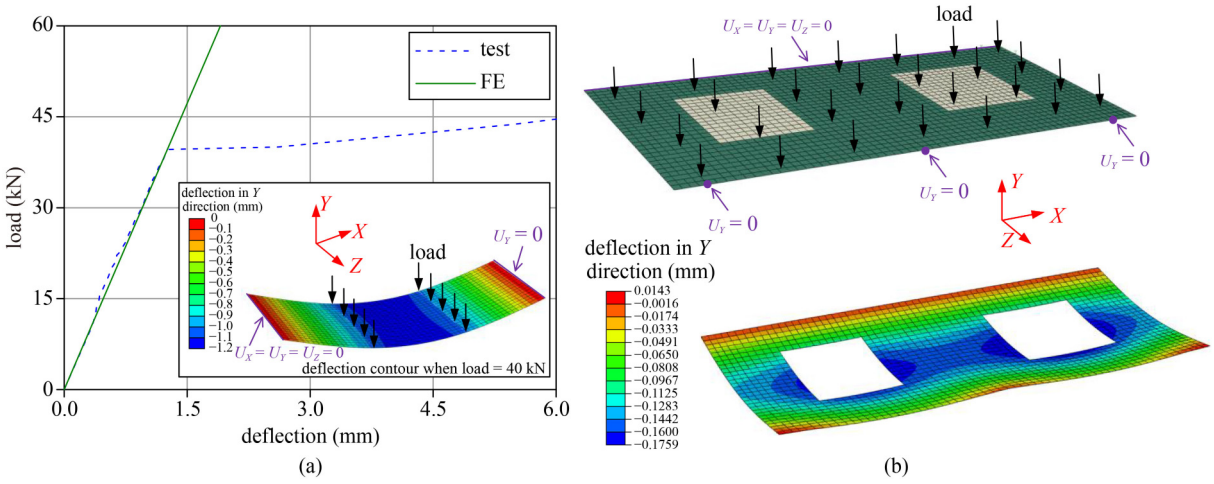

Fig. 10 FE model and the analysis result: (a) comparison of the test and FE results in Ref. [12]; (b) FE model of the FC counterpart of SP-6280-2-3 (wind load = 1 kN/m^2). (Reprinted from Magazine of Concrete Research, 72(3), Huang J, Jiang Q, Chong X, Ye X, Wang D, Experimental study on precast concrete sandwich panel with cross-shaped GFRP connectors, 149–162, Copyright 2020, with permission from ICE Publishing.)

4.3.2 Degree of composite action of the specimens

Generally, for a PCSP, the degree of composite action primarily consists of degree of composite action in terms of initial stiffness (DCA_{is}) and degree of composite action in terms of ultimate strength (DCA_{us}). They are calculated based on the initial stiffness or the load carrying capacity of the PCSPs [12,25]. For the specimens in this study, owing to the termination of test on or before the initial yielding stage, the load carrying capacity remained unclear, and DCA_{us} could not be calculated. Moreover, the initial stiffness of the specimens was difficult to calculate because the deformation of the PCSP was different with that of a one-way element. Therefore, in this study, referring to Ref. [18], the degree of composite action in terms of deflection (DCA_d) was adopted, and its equation is as follows:

$$DCA_d = \frac{\Delta_{non} - \Delta_{test}}{\Delta_{non} - \Delta_{fully}} \times 100\% , \quad (2)$$

where Δ_{test} is the deflection of the tested PCSP at a selected load level, Δ_{fully} is the corresponding deflection of the fully composite PCSP, and Δ_{non} is the corresponding deflection of the non-composite PCSP.

In this study, the investigating load level was 1 kN/m^2. The obtained DCA_d values are shown in Table 4. All specimens exhibited considerably high DCA_d values, which were larger than 60%. Moreover, increasing the bottom support number (i.e., reducing bottom support spacing) decreased the DCA_d value. A possible reason was that the increase in the bottom support number could also facilitate a significant reduction in the deflections of the fully composite and non-composite counterparts. Here, from the results of SP-4980-0-2 and SP-4980-0-3, a decrease of 21% was observed on DCA_d (i.e., from 78.87% to 61.68%) when the bottom supports were increased from 2 to 3. Moreover, for the results of SP-8020-2-3 and SP-8020-2-4, a decrease of 7% was observed on DCA_d (i.e., from 67.41% to 63.02%) when the bottom supports were increased from 3 to 4.

5 Conclusions

A comprehensive study was performed on the pull-out and shear performance of a bar-type BFRP connector, and the out-of-plane flexural performance of the façade PCSP with different lengths, opening conditions and boundary conditions. The following were the conclusions of the study.

1) The bar-type BFRP connector has a good potential to achieve a reliable anchorage system in PCSPs, although the exposed temperature would affect the pull-out capacity. Generally, through increasing the temperature from –20 to 60 °C, the pull-out capacity exhibits a decrease of 50.8%.

2) The bar-type BFRP connector can provide considerable stiffness and capacity based on the direct shear test results, indicating a good potential to achieve a partially composite action in the PCSP.

3) Increasing the bottom support number (i.e., reducing bottom support spacing) would improve the cracking load and the slope of the load–deflection curve of the PCSP. The opening condition would particularly affect the crack pattern of the PCSP.

4) All PCSP specimens reflected a degree of composite action in terms of deflection (DCA_d) higher than 60%, which was a partially composite type.

Acknowledgements The research in this paper was financially supported by the National Natural Science Foundation of China (Grant No.

51878233), the Fundamental Research Funds for the Central Universities (No. JZ2021HGTA0164), from the Key Research and Development Project of Anhui Province, China (No. 202104a07020022), and from Anhui Provincial Natural Science Foundation (No. 2208085QE172).

References

1. Committee PCI. PCI Design Handbook. 7th ed. Chicago, IL: Precast/Prestressed Concrete Institute, 2010
2. Committee PCI. State of the art of precast/prestressed concrete sandwich wall panels. PCI Journal, 2011, 56(2): 131−176
3. Bush T D, Stine G L. Flexural behavior of composite precast concrete sandwich panels with continuous truss connectors. PCI Journal, 1994, 39(2): 112−121
4. Kinnane O, West R, Hegarty R O. Structural shear performance of insulated precast concrete sandwich panels with steel plate connectors. Engineering Structures, 2020, 215: 110691
5. Salmon D C, Tadros M K, Culp T. A new structurally and thermally efficient precast sandwich panel system. PCI Journal, 1994, 39(4): 90−101
6. Woltman G, Tomlinson D, Fam A. Investigation of various GFRP shear connectors for insulated precast concrete sandwich wall panels. Journal of Composites for Construction, 2013, 17(5): 711−721
7. Choi K B, Choi W C, Feo L, Jang S J, Yun H D. In-plane shear behavior of insulated precast concrete sandwich panels reinforced with corrugated GFRP shear connectors. Composites. Part B, Engineering, 2015, 79: 419−429
8. Pantelides C P, Surapaneni R, Reaveley L D. Structural performance of hybrid GFRP/steel concrete sandwich panels. Journal of Composites for Construction, 2008, 12(5): 570−576
9. Jawdhari A, Fam A, Kadhim M. Thermal bowing of reinforced concrete sandwich panels using time-domain coupled-field finite element analysis. Engineering Structures, 2022, 252: 113592
10. Norris T G, Chen A. Development of insulated FRP-confined Precast Concrete Sandwich panel with side and top confining plates and dry bond. Composite Structures, 2016, 152: 444−454
11. Chen A, Norris T G, Hopkins P M, Yossef M. Experimental investigation and finite element analysis of flexural behavior of insulated concrete sandwich panels with FRP plate shear connectors. Engineering Structures, 2015, 98: 95−108
12. Huang J, Jiang Q, Chong X, Ye X, Wang D. Experimental study on precast concrete sandwich panel with cross-shaped GFRP connectors. Magazine of Concrete Research, 2020, 72(3): 149−162
13. Huang J Q, Dai J G. Direct shear tests of glass fiber reinforced polymer connectors for use in precast concrete sandwich panels. Composite Structures, 2019, 207: 136−147
14. Lameiras R, Barros J, Valente I B, Azenha M. Development of sandwich panels combining fibre reinforced concrete layers and fibre reinforced polymer connectors. Part I: Conception and pull-out tests. Composite Structures, 2013, 105: 446−459
15. Dutta D, Jawdhari A, Fam A. A new studded precast concrete sandwich wall with embedded glass-fiber-reinforced polymer channel sections: Part 1, experimental study. PCI Journal, 2020, 65(3): 78−99
16. Jawdhari A, Fam A. A new studded precast concrete sandwich wall with embedded glass-fiber-reinforced polymer channel sections: Part 2, finite element analysis and parametric studies. PCI Journal, 2020, 65(4): 51−70
17. Frankl B A, Lucier G W, Hassan T K, Rizkalla S H. Behavior of precast, prestressed concrete sandwich wall panels reinforced with CFRP shear grid. PCI Journal, 2011, 56(2): 42−54
18. Hassan T K, Rizkalla S H. Analysis and design guidelines of precast, prestressed concrete, composite load-bearing sandwich wall panels reinforced with CFRP grid. PCI Journal, 2010, 55(2): 147−162
19. Kazem H, Bunn W G, Seliem H M, Rizkalla S H, Gleich H. Durability and long term behavior of FRP/foam shear transfer mechanism for concrete sandwich panels. Construction & Building Materials, 2015, 98: 722−734
20. Kim J H, You Y C. Composite behavior of a novel insulated concrete sandwich wall panel reinforced with GFRP shear grids: Effects of insulation types. Materials (Basel), 2015, 8(3): 899−913
21. Choi I, Kim J H, Kim H R. Composite behavior of insulated concrete sandwich wall panels subjected to wind pressure and suction. Materials (Basel), 2015, 8(3): 1264−1282
22. Choi I, Kim J H, You Y C. Effect of cyclic loading on composite behavior of insulated concrete sandwich wall panels with GFRP shear connectors. Composites. Part B, Engineering, 2016, 96: 7−19
23. Shams A, Horstmann M, Hegger J. Experimental investigations on textile-reinforced concrete (TRC) sandwich sections. Composite Structures, 2014, 118: 643−653
24. O'Hegarty R, West R, Reilly A, Kinnane O. Composite behaviour of fibre-reinforced concrete sandwich panels with FRP shear connectors. Engineering Structures, 2019, 198: 109475
25. Huang J Q, Dai J G. Flexural performance of precast geopolymer concrete sandwich panel enabled by FRP connector. Composite Structures, 2020, 248: 112563
26. Rolland A, Quiertant M, Khadour A, Chataigner S, Benzarti K, Argoul P. Experimental investigations on the bond behavior between concrete and FRP reinforcing bars. Construction and Building Materials, 2018, 173: 136−148
27. Yoshitake I, Tsuda H, Itose J, Hisabe N. Effect of discrepancy in thermal expansion coefficients of CFRP and steel under cold temperature. Construction & Building Materials, 2014, 59: 17−24
28. Zhang J, Huang Z, Li Z, Yan P, Zhang P. Temperature fields of external walls of different thermal insulation placements. Journal of Harbin Engineering University, 2009, 30(12): 1356−1365 (In Chinese)
29. Signorini C, Sola A, Malchiodi B, Nobili A, Gatto A. Failure mechanism of silica coated polypropylene fibres for Fibre Reinforced Concrete (FRC). Construction & Building Materials, 2020, 236: 117549
30. Zhou Z, Qiao P. Bond behavior of epoxy-coated rebar in ultra-high performance concrete. Construction & Building Materials, 2018, 182: 406−417
31. Choi I, Kim J H, Kim D W, Park J S. Effects of grid-type shear connector arrangements used for insulated concrete sandwich wall panels with a low aspect ratio. Journal of Building Engineering, 2022, 46: 103754

32. Hou H, Wang W, Qu B, Dai C. Testing of insulated sandwich panels with GFRP shear connectors. Engineering Structures, 2020, 209: 109954
33. Hibbit H D, Karlsson B I, Sorensen E P. ABAQUS User Manual, Version 6.12. Providence, RI: Simulia, 2012
34. ACI 318M-05. Building Code Requirements for Structural Concrete and Commentary. Farmington Hills, MI: American Concrete Institute, 2005